Electrochemical Performance of Mixed Redox-Active Organic Molecules in Redox Flow Batteries

Kiana Amini, Yan Jing, Jinxu Gao, Jordan D. Sosa, Roy G. Gordon, Michael J. Aziz[z]

K. Amini, J.D. Sosa, M. J. Aziz, Harvard John A. Paulson School of Engineering and Applied Sciences, 29 Oxford Street, Cambridge, Massachusetts 02138, USA.

Y. Jing, J. Gao, R. G. Gordon, Department of Chemistry and Chemical Biology, Harvard University, 12 Oxford Street, Cambridge, Massachusetts 02138, USA.

[z]Corresponding Author: maziz@harvard.edu (Michael J. Aziz).

Abstract

Designing electrolytes based on mixture of different organic redox active molecules brings the opportunity of enhancing the volumetric energy density of flow batteries and removes the requirement of high solubility for individual organic species in the mixture. In the present work, we conduct computational and experimental analysis to investigate the electrochemical performance of mixed redox-active organic molecules. A zero-dimensional transient model is employed to investigate the changes in the half-cell potential and the concentrations and partial currents of individual redox reactions in a mixture of organic molecules over time. The model demonstrates the effects of individual properties of species such as kinetic rate constants, mass transfer coefficients, concentration ratios and standard redox potentials and reports the effect of energy-losing homogenous chemical redox reaction on the voltage efficiency and concentration ratios of the mixed species. Pairs of anthraquinone negolyte species were selected for an experimental case study. A mixture of 2,6-N-TSAQ and 2,6-DHAQ showed 40% increase in the volumetric energy density compared to the performance of 2,6-DHAQ alone. Based on the results of the experimental and computational analysis, we propose guidelines for the design of suitable mixed redox-active organic species.

Introduction

Renewable sources of energy such as solar and wind are attractive options for production of clean and sustainable electricity. Nevertheless, the intermittent nature of these resources challenges their reliability and disrupts their continuous availability [1]. This challenge can be addressed by employing a reliable, cost-effective and efficient energy storage technology capable of storing and smoothly releasing the energy as needed [2]. Energy Storage systems with long discharge duration are particularly useful for regulating intermittent renewable sources because it allows for a longer period of time over which the stored energy can be discharged to supplement or replace power dropouts from the intermittent renewable source. Redox flow batteries (RFBs) are attractive

technologies with a unique architecture that has showed promise for large-scale energy storage applications. In RFBs, in which the electrolyte containing the redox active species is stored in external tanks and is continuously pumped to the electrochemical cell stack, the stack (power component) and the electrolyte (energy capacity component) can be independently and flexibly designed and scaled up [3].

Among different types of RFBs, aqueous organic-based RFBs have gained a lot of attention due to the possibility of tuning their properties by modifying their molecular structures. To date, organic species with variety of core structures such as quinones [4], ferrocenes [5], viologens [6,7], phenazines [8,9] and alloxazines [10] have been investigated [11]. The solubility, stability and the redox potential of these molecules have been tuned by modifying their chemical structures with different functional groups. For example, anthraquinones modified by a single [12] or double [13] carboxylate-capped methyl-branched side chain exhibited high chemical stability characterized by a capacity fade rate < 0.03%/day with a redox potential of approximately -0.47 V vs. SHE (pH 14) and have been operated at concentrations as high as 1.1 M. In contrast, anthraquinones modified by bis(azanetriyl))tetrakis(propane-1-sulfonate) (2,6-N-TSAQ) [14] chains showed a much more negative redox potential of -0.63 V vs. SHE with a fade rate of 0.025%/day but a lower operating concentration, defined as 0.1 M lower than the compound's maximum solubility to assure no precipitates are forming locally in the cell, of only 0.35 M. 2,6-Dihydroxyanthraquinone (2,6-DHAQ) [15], with a lower molecular weight, which correlates with a lower mass production cost, also possesses quite a negative redox potential of -0.68 V vs. SHE but shows high fade rates in the range of 4-8%/day. Consequently, designing a molecule that combines all the desirable properties of high stability and solubility, low cost and proper negative/positive redox potential has been a challenge.

In the present work, we investigate the design of an aqueous electrolyte that contains a mixture of organic-based redox active species, resulting in a flow battery with multiple redox couples undergoing charge and discharge. Such an approach, with a correct choice of redox active molecules for the mixture, can bring multiple advantages. Firstly, by employing multiple redox-active species dissolved at their highest operating concentration, one may increase the volumetric energy density of organic-based RFBs. Indeed, RFBs are designed for stationary energy storage applications and their volumetric energy density does not need to match that of lithium-ion batteries [4]. Nevertheless, in order to penetrate the market for residential and small-scale commercial customers, enhancement in the volumetric energy density and thus reduction in the system size is important [16]. Additionally, when the cost/kWh of the electrolytes and the cost/kW of the power stack become low enough for the flow battery to be competitive, the cost of the electrolyte storage tanks themselves is no longer negligible. Consequently, increasing the volumetric energy density of aqueous organic-based RFBs would enhance their competitiveness both in terms of system sizes and cost. The concept of employing multiple redox active species could be equally used for improving the energy density of metal-based systems such as all-

vanadium RFBs, as is shown in two prior reports [17,18] . However, designing appropriate redox active mixtures with metal-based species is a more complicated task. Firstly, in a system such as all-vanadium RFB, due to high rates of vanadium cross-over, a rebalancing system needs to be employed [19]. As such, mixing vanadium with other metals would make the recovery of the electrolyte significantly complicated. Additionally, for designing suitable mixed redox active mixtures, tunability of the electrochemical properties of the redox active species is highly beneficial, but this feature is unique to organic-based compounds.

In addition to improving the energy density, mixing multiple redox active molecules would open up the possibility of employing low-solubility chemistries in RFBs. The tunability of organic species results in an abundance of possible molecular structures and selecting the best candidate from such a list is not a simple task [20]. To accelerate the selection, synthesis and characterization of new organic molecules, several minimum requirements are set. For example, as a rule of thumb, a minimum solubility of 0.5 M for an anthraquinone (with 2 electron transfer) would be desirable and compounds with lower solubility would not typically be selected for further characterization. However, if such low-solubility compounds can be utilized in a mixture, individual solubility would be removed as one of the hard requirements and consequently low-solubility redox-active species are brought back into the material discovery cycle. It is possible that the future grid-scale organic-based redox flow batteries are made up of multiple low-solubility organic species that could otherwise bring combined advantage of low cost and high stability.

In the following sections, we report the results of a zero-dimensional transient model for the performance of a system of mixed redox-active species. Note that the mixed redox active species are independent compounds with distinct properties, rather than different oxidation states of the same compound as described in the literature. [21]. The changes in the temporal concentration profile, partial currents and half-cell potential of a mixture of two redox reactions were studied and the effects of individual properties of each compound such as their kinetic and mass transfer rates, redox potentials and concentration ratios are discussed. Additionally, the effect of the homogenous redox reaction between the mixed redox active species on the cell's performance is investigated at various states of charge (SOC) and redox potential separations. Following this computational analysis, we report the results of an experimental case study with selected anthraquinones to investigate complications such as chemical degradation and precipitation. The present modeling scheme and experimental case study can be used as a guide for the design and thorough investigation of new organic-based redox active mixtures.

The Model

The present modeling scheme describes the electrochemical performance of a mixed redox active solution comprised of two independent redox reactions occurring on the same electrode:

$$A^{m+} + ze^- \leftrightarrow A^{(m-z)+} \qquad E_0^A,\ I_A \tag{1}$$

$$B^{m'+} + z'e^- \leftrightarrow B^{(m'-z')+} \qquad E_0^B,\ I_B \tag{2}$$

where E_0^i, I_i are the standard reduction potential and the partial current of $i = \{A: A^{(m-n)+}, A^{m+}\}, \{B: B^{(m'-z')+}, B^{m'+}\}$, respectively, where in this example m and m' is 2 and z and z' is 1. When a total current of I is applied to the electrode to galvanostatically reduce the compounds, the applied current is distributed between the two reactions depending on their individual properties, yielding partial currents of I_A and I_B. Thus:

$$I = I_A + I_B \tag{3}$$

The properties that would affect the distribution of partial currents are the equilibrium potentials of each reaction, the surface and bulk concentrations of reduced and oxidized form of both compounds ($C_{i,s}, C_{i,b}$), the exchange currents ($I_{0,i}$) and the mass transfer coefficients ($k_{m,i}$) of each species. In this modeling scheme, we assume that the reduced and the oxidized form of each ion has the same mass transfer coefficient (e.g., $k_{m,A^{m+}} = k_{m,A^{(m-z)+}}$) and the forward and reverse electrochemical reactions has the same exchange current (e.g., $I_{O,i}$ for reaction i=A,B). At each time step (t_n), the partial current of each reaction is calculated from the mass-transfer controlled Butler-Volmer equation:

$$I_A(t_n) = I_{O,A}\left[\frac{C_{A^{(m-z)+},s}(t_n)}{C_{A^{(m-z)+},b}(t_n)} exp\left(\frac{\alpha z F}{RT}\left(E_{cell}(t_n) - E_{eq}^A\right)\right) - \frac{C_{A^{m+},s}(t_n)}{C_{A^{m+},b}(t_n)} exp\left(-\frac{(1-\alpha) z F}{RT}\left(E_{cell}(t_n) - E_{eq}^A\right)\right)\right] \tag{4}$$

$$I_B(t_n) = I_{O,B}\left[\frac{C_{B^{(m'-z')+},s}(t_n)}{C_{B^{(m'-z')+},b}(t_n)} exp\left(\frac{\alpha' z' F}{RT}\left(E_{cell}(t_n) - E_{eq}^B\right)\right) - \frac{C_{B^{m+},s}(t_n)}{C_{B^{m+},b}(t_n)} exp\left(-\frac{(1-\alpha') z' F}{RT}\left(E_{cell}(t_n) - E_{eq}^B\right)\right)\right] \tag{5}$$

where α and α' is the charge transfer coefficient, z is the number of electrons transferred, F is the Faraday's constant, and R and T are the universal gas constant and the absolute temperature, respectively. $E_{cell}(t_n)$ is the half-cell electrode potential (versus SHE) resulting from the total applied current I_t.

The equilibrium potentials E_{eq}^i in Equations (4) and (5) are calculated at each time step according to the Nernst Equation using activities (a_i) of each species:

$$E_{eq}^A = E_0^A + \frac{RT}{zF} \exp\left(\frac{a_{A^{m+},b}(t_n)}{a_{A^{A^{(m-z)+},b}}(t_n)}\right) \tag{6}$$

$$E_{eq}^{B} = E_0^{B} + \frac{RT}{zF}\exp\left(\frac{a_{B^{m+},b}(\mathrm{t_n})}{a_{B^{(m'-z')+},b}(\mathrm{t_n})}\right) \quad (7)$$

Activities are related to concentration using $a_i = \gamma_i C_i$, where γ_i is the activity coefficient of species i. In this model, all activity coefficients are assumed to be 1. The bulk concentrations at each time step are calculated according to the transient mass-balance equations:

$$C_{i,b}\,(t_{n+1}) \;=\; C_{i,b}\,(t_n) - \frac{I_i(t_n)dt}{VzF} \qquad (8)$$

where V is the electrolyte volume; this assumes that the electrolyte volume is always well-mixed. Given that there are four redox-active species present in the mixture, Equation (8) yields 4 equations for species concentrations. The surface concentration of each species is related to the bulk concentration by balancing the rate of the individual reactions with their mass-transfer rates, characterized by mass-transfer coefficients $k_{m,i}$ (where $i = A, B$) to (or from) the electrode. For example, for A^{m+} and $A^{(m-z)+}$ ions we have:

$$zFk_{m,A}\left(C_{A^{(m-z)+},b} - C_{A^{(m-z)+},S}\right) = \; I_{O,A}\;\left[\frac{C_{A^{(m-z)+},S}(t_n)}{C_{A^{(m-z)+},b}\,(t_n)}\exp\left(\frac{\alpha zF}{RT}\left(E_{cell}(t_n) - E_{eq}^{A}\right)\right) - \frac{C_{A^{m+},S}(t_n)}{C_{A^{m+},b}\,(t_n)}\exp\left(-\frac{(1-\alpha)zF}{RT}\left(E_{cell}(t_n) - E_{eq}^{A}\right)\right)\right] \quad (9)$$

$$zFk_{m,A}\left(C_{A^{m+},b} - C_{A^{m+},S}\right) = -\; I_{O,A}\;\left[\frac{C_{A^{(m-z)+},S}(t_n)}{C_{A^{(m-z)+},b}\,(t_n)}\exp\left(\frac{\alpha zF}{RT}\left(E_{cell}(t_n) - E_{eq}^{A}\right)\right) - \frac{C_{A^{m+},S}(t_n)}{C_{A^{m+},b}\,(t_n)}\exp\left(-\frac{(1-\alpha)zF}{RT}\left(E_{cell}(t_n) - E_{eq}^{A}\right)\right)\right] \quad (10)$$

By assuming $\alpha = 0.5$, for simplicity, and by combining Equations (9) and (10), the surface concentrations of A^{m+} and $A^{(m-z)+}$ ions are related to their bulk concentrations at each time step, yielding:

$$C_{A^{m+},S}\,(\mathrm{t_{n+1}}) = \frac{A_c\,C_{A^{m+},b}(t_{n+1}) + (1+A_c)C_{A^{(m-z)+},b}(t_{n+1})}{1+A_a+A_c} \qquad (11)$$

$$C_{A^{(m-z)+},S}\,(\mathrm{t_{n+1}}) = \frac{A_a\,C_{A^{(m-z)+},b}(t_{n+1}) + (1+A_a)C_{A^{m+},b}(t_{n+1})}{1+A_a+A_c} \qquad (12)$$

where A_a and A_c coefficients are:

$$A_a = \frac{I_{0A}}{Fk_{m,A}C_{A^{(m-z)+},b}(t_{n+1})}\exp\left(\frac{0.5F\left(E_{cell}-E_{eq}^{A}\right)}{RT}\right) \qquad (13)$$

$$A_c = \frac{I_{0A}}{Fk_{m,A}C_{A^{m+},b}(t_{n+1})} \exp\left(-\frac{0.5F\left(E_{cell}-E_{eq}^{A}\right)}{RT}\right) \quad (14)$$

Equations (9) – (14) can be similarly written for compound B, assuming $\alpha' = 0.5$.

Based on this transient 0-dimensional model there are 11 unknown parameters calculated at each time step: 4 bulk concentrations ($C_{i,b}$), 4 surface concentrations ($C_{i,s}$), half-cell redox potential (E_{cell}) and partial currents I_A, I_B. These unknowns are found from the 11 independent Equations described above comprising Equation (3) with a known total applied current, the Butler-Volmer Equations (Equations (4) and (5)), four mass-balance equations (Equation (8) written for the 4 ions) and the four mass-transfer balanced with kinetic rate Equations (Equations (9)-(10) and the equivalents for compound B). The results of this model are shown in Figures 1 – 4. For the cases where voltage efficiency or voltage of a cell is shown, the posolyte is assumed to be ferrocyanide/ferricyanide redox couple with redox potential of 0.47 V vs. SHE and 100 mV overpotential (0.57 V for charge and 0.37 V for discharge).

We additionally explored the effect of the homogenous redox reaction between the mixed redox active species on the cell's performance. Having reactions (1) and (2) occurring in the same reservoir, a chemical reaction between the mixed redox active species can occur as long as the oxidized form of one species is present simultaneously with the reduced form of the other species:

$$A^{m+1} + B^{m} \leftrightarrow A^{m} + B^{m+1} \quad (15)$$

The rates of the forward and reverse reactions depend on the concentrations and rate constants for the specific redox-active species studied. In the present study, we assume that the battery is charged to a range of SOC values at a rate sufficiently fast to avoid being influenced by the chemical reaction during charge or discharge. However, we assume sufficient time has passed after charging or discharging is completed for the chemical reaction to occur and reach equilibrium. Given the standard reduction potential of the compounds A and B, the equilibrium constant (K) for the homogenous redox reaction can be found:

$$\Delta E^0 = E_A^o - E_B^o = \frac{0.059\,V}{z} log_{10}\,K; \quad (16)$$

$$K = 10^{\frac{z\Delta E^0}{0.059}}. \quad (17)$$

Consequently, the equilibrium concentrations are found:

$$K = \frac{C_{A^{m},b}^{eq}\, C_{B^{m+1},b}^{eq}}{C_{A^{m+1},b}^{eq}\, C_{B^{m},b}^{eq}} \quad (18)$$

In section 5, we find the concentrations of the A and B at a certain SOC and thus find the reaction quotient at this SOC:

$$Q = \frac{C_{A^{m},b}\, C_{A^{m+1},b}}{C_{A^{m+1},b}\, C_{B^{m},b}} \quad (19)$$

The forward chemical reaction ($Q < K$) or the backward chemical reaction ($Q > K$) shown in Eq. (15) consequently would bring species concentrations to equilibrium (Equation (18)). We thus find the concentrations of A and B at various SOC with and without the occurrence of homogenous redox reaction and compare the concentration ratios and the resulting voltage efficiency loss as a function of SOC and of separation between the standard redox potentials of compounds A and B.

Computational Results

To better understand the effect of the individual parameters on the concentration evolution and partial current distribution of compounds A and B, we first investigate a mixed redox active negolyte (negative electrolyte) undergoing reactions shown in Equations (1) and (2), in which all the properties of A and B are assumed to be equal (see **Table 1**), except for their standard redox potentials, which is 100 mV more negative for compound B compared to the compound A ($E_0^A = -0.5\,V\ vs.SHE, E_0^B = -0.6\,V\ vs.SHE$). Kinetic and mass-transfer parameters differing by orders of magnitude, as well as lower and higher potential separations, are discussed subsequently. **Figure 1a** presents the partial currents of A and B as well as the total current during the electrochemical reduction reaction that occurs when the cell is charged. Because compound A possesses an equilibrium reduction potential less negative compared to that of compound B, it is easier to reduce A^{2+} compared to reducing B^{2+}. As such, the total current (0.2 A) is distributed between A and B in a way that A initially takes up a higher share (~0.15 A) from the total applied current compared to compound B (~0.05 A) as is shown in Figure 1a. As the charging reactions go toward completion, the concentration of reactant A^{2+} is depleted and eventually A^{2+} is completely consumed, at which point the entire applied current goes towards reducing B^{2+} with a more negative redox potential. The opposite trend exists for the oxidation reaction that occurs during discharging the cell: the oxidation of B^{+} initially exhibits the higher partial current until the compound B is essentially fully oxidized (see **Figure 1b**).

Table 1: Operating conditions and constants used in Figures 1-3.

Total applied current (I)	0.2 A
Exchange current for both reactions A and B ($I_{O,A}$, $I_{O,B}$)	5E-3 A
Mass transfer coefficient of A and B ($k_{m,A}, k_{m,B}$)	1E-5 ms^{-1}
Initial bulk concentration of oxidized A and B ($C_{A^{2+},b}(t=0), C_{B^{2+},b}(t=0)$)	0.1 M
Initial bulk concentration of reduced A and B ($C_{A^{+},b}(t=0), C_{B^{+},b}(t=0)$)	1E-4 M
Electrolyte volume (V)	5E-6 m^3
Faradays Constant (F)	96485 C mol^{-1}
Temperature (T)	298 K
Universal gas constant (R)	8.314 J mol^{-1} K^{-1}
Electron transfer number (z for both reactions)	1
Charge transfer coefficient for both reactions (α)	0.5

The change in the concentration of all species in the half-cell over a cycle is presented in **Figure 1c** (reduction) and **Figure 1d** (oxidation). Consistent with the partial currents, we can see that during the reduction reaction, initially the rate of the change in the consumption of A^{2+} is faster than the rate of the consumption of B^{2+}, until the concentration of A^{2+} is completely depleted (when ≈70 coulombs have been reacted). From this point forward, the rate of the consumption of B^{2+} is accelerated, as evidenced by the slope change found for B^{+} and B^{2+} concentrations in Figure 1c. As expected, an opposite trend is found for the concentration changes during the oxidation (**Figure 1d**). The resulting half-cell potential of the cell is shown in **Figure 1e**, clearly showing two plateaus in the voltage profile for both the charge and the discharge phases. By combining the results of concentration, partial current and the voltage profile, we can find that both reactions of A and B occur simultaneously during the first voltage plateau, with reaction A possessing a larger rate during reduction and reaction B possessing a larger rate during oxidation. The step to the second plateau in the voltage profile during reduction or oxidation occurs exactly at the time where the concentration of A or B is completely depleted, respectively.

Building upon the understanding gathered from Figure 1 for a fixed potential separation between A and B, we are now positioned to investigate the electrochemical performance of the compounds with different magnitude of separation between their redox potentials. **Figure 2** shows the concentration changes and the partial current values during reduction of compound A and B with

the properties shown in Table 1, but for the case where the potential separation changes from 0 mV to 400 mV ($E_0^A = -0.5\,V\ vs.\ SHE, E_0^B = -0.5, -0.55, -0.6, -0.65, -0.7, -0.8, -0.9 V\ vs.\ SHE$).

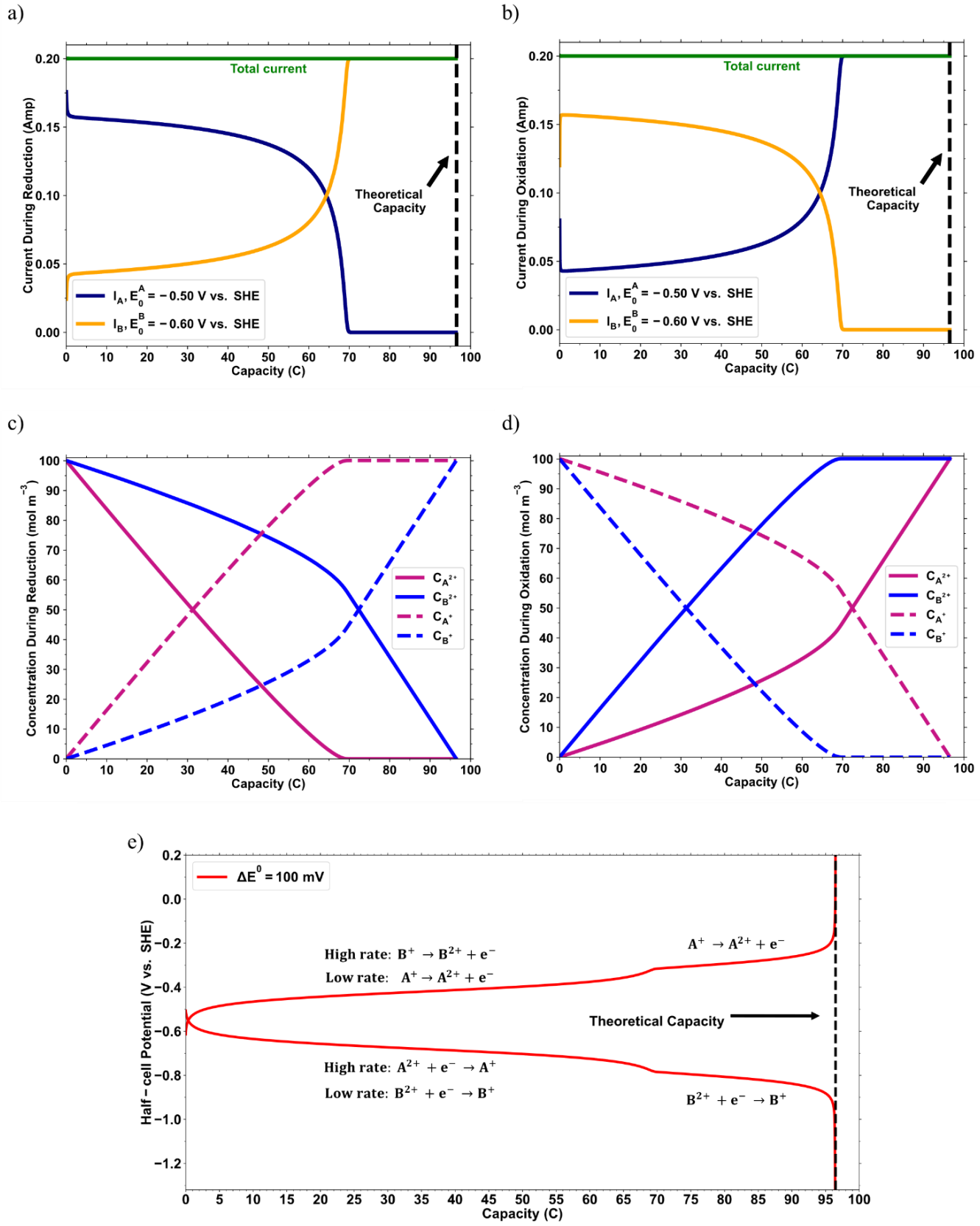

Figure 1 Simulated properties of a mixture of redox active species of A and B with properties listed in Table 1 and redox potential of $E_0^A = -0.5\,V\ vs.\ SHE\ and\ E_0^B = -0.6\,V\ vs.\ SHE$. a) partial currents of A and B during reduction and b) oxidation. c) Concentration of the reduced and oxidized forms of A and B during reduction and d) oxidation and e) the half-cell potential of the system versus capacity during operation.

As shown in **Figure 2**, in the absence of any potential separation between compound A and B, the partial currents are distributed equally between A and B, and thus the concentration of A^{2+} and B^{2+} depletes with equal rates. As the potential separation becomes bigger, the portion of the total current allocated to the reaction with more positive redox potential (compound A) becomes higher and thus A^{2+} is consumed faster than B^{2+}. At potential separation of 400 mV, the entire applied current first would be allocated to reducing compound A^{2+} and then once A^{2+} is completely depleted, reduction of the second compound begins.

The concentration plots shown in **Figure 2c** and **2d** reveal important information regarding the co-existence of the reduced and oxidized form of each species during the reaction time. At large potential separations (> 200 mV), it is evident that the oxidized form of the compound with a more positive redox potential (compound A^{2+}), barely co-exist with the reduced form of the compound with a more negative redox potential (compound B^{+}). This is because at larger potential separations, compound A is essentially completely reduced by the time the reduction of B^{2+} begins. Consequently, within the context of this 0D model for an electrolyte that is always well-mixed, the homogenous redox reaction (reaction (15)) does not occur for mixtures with large potential separations. At a lower potential separation, depending on the state of charge (SOC) of the battery, the oxidized and reduced form of both species co-exist to a significant extent in the same electrolyte as is evident from Figure 2. The enhanced role of reaction (15) as the redox potential separation becomes smaller is investigated later.

The voltage-capacity profiles for different potential separations are shown in **Figure 3a**. It can be seen that as the potential separation becomes bigger, the presence of two plateaus in the voltage profile becomes more evident. Additionally, the second plateau appears earlier during the charge or discharge, and it approaches the point at which half of the capacity is accessed. This is because as the potential separation becomes higher, the reduction of A^{2+} and B^{2+} occurs more separately (rather than simultaneously). Because we have mixed the two compounds in equal concentrations in this example, the step in the voltage plateau occurs when half of the capacity is delivered. This observation is consistent with the partial current and concentration trends at different potential separations.

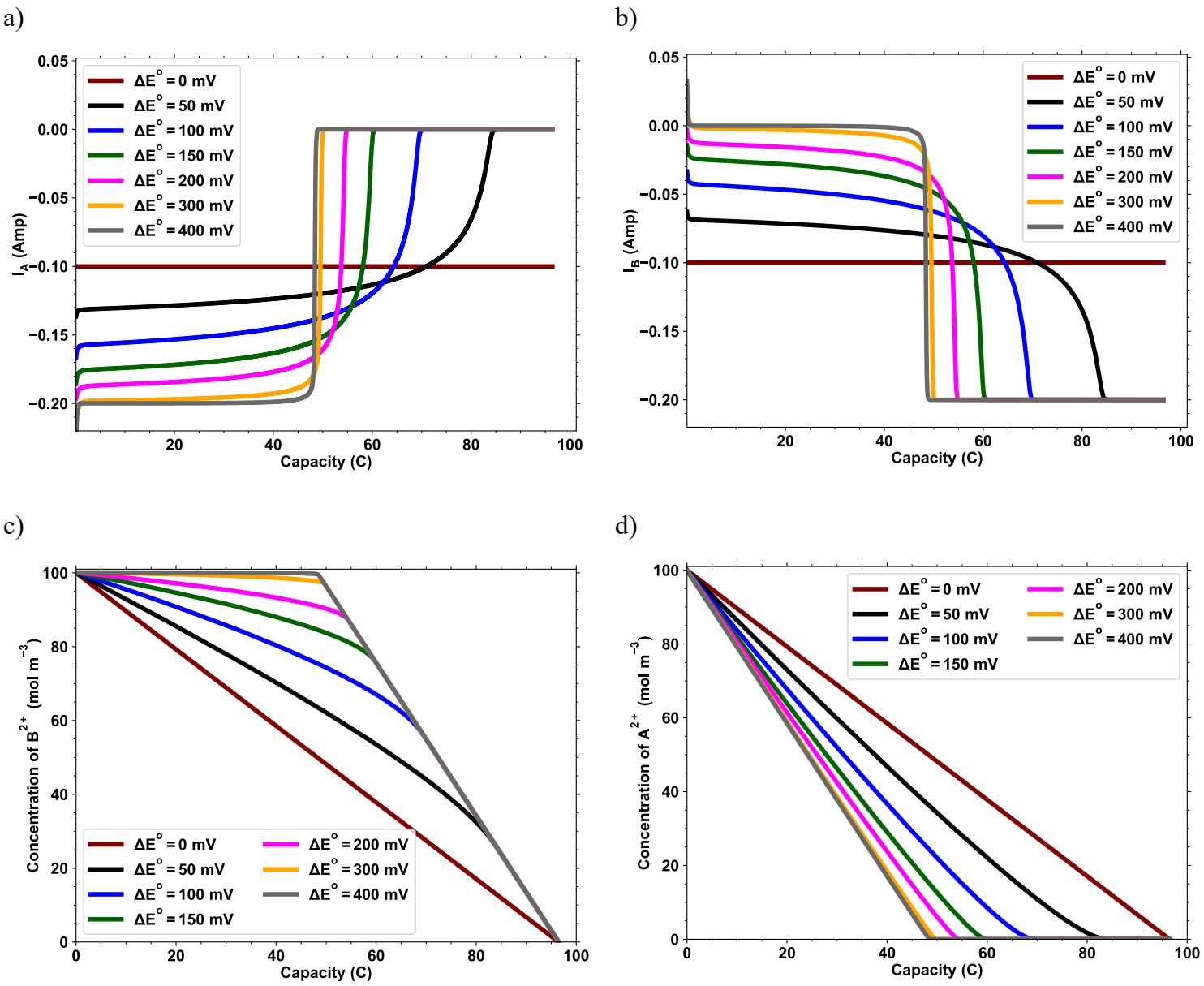

Figure 2 Simulated properties of a mixture of redox active species of A and B with properties listed in Table 1 and redox potential of $E_0^A = -0.5\,V\ vs.SHE$ and $E_0^B = -0.5, -0.55, -0.6, -0.65, -0.7, -0.8, -0.9 V\ vs.SHE$. Partial currents of a) compound A and b) compound B during reduction. Concentration of c) the oxidized form of A (A^{2+}) and d) the oxidized form of B (B^{2+}) during reduction.

One finding from the voltage-capacity profile at different potential separations is the resulting change in the average half-cell potential of the system (averaged from charge and discharge half-cell potential profiles). In the simple example where two compounds with the same redox potentials of -0.5 V vs. SHE are mixed, the entire 96 C capacity is delivered at the average half-cell potential of -0.5 V vs. SHE. In contrast, when compound A, with redox potential of -0.5 V vs. SHE, is mixed with a compound that has a more negative redox potential then the average half-cell potential becomes more negative. Consequently, a battery constructed from such a mixture yields a higher cell voltage. **Figure 3b** shows that the gain in the cell voltage can be as high as 200 mV when compound A with a redox potential of -0.5 V vs. SHE is mixed with compound B with a redox potential of -0.9 V vs. SHE (400 mV separation). Indeed, for achieving a high cell-voltage battery we ideally want to deliver the entire capacity with the compound that has the more extreme redox potential. But if such a compound has a lower solubility than desired, the present results show that it can still be utilized in a mixture. Essentially, low-solubility redox active species is still useful if they have large negative or positive redox potentials because they can be used in mixtures of redox active species to increase the cell voltage of the battery.

a)

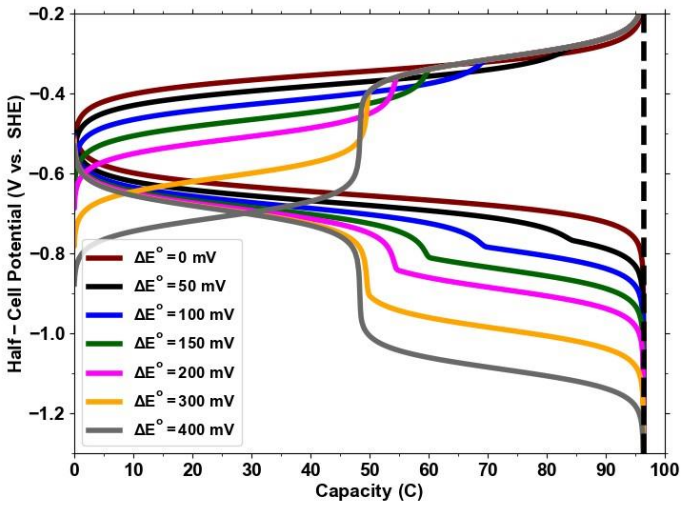

b)

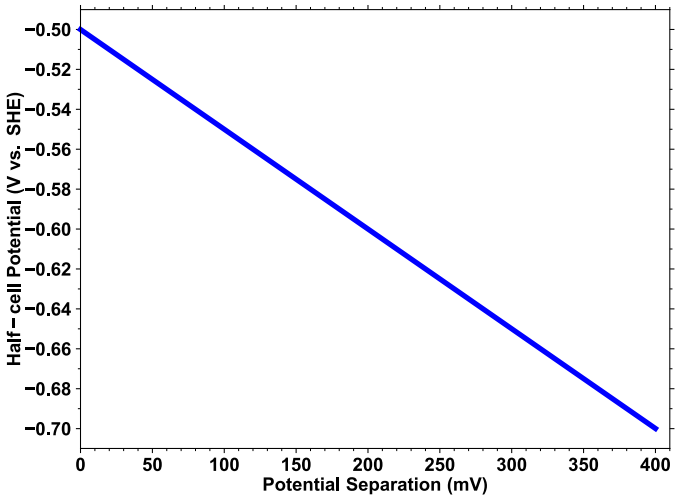

Figure 3 Simulated properties of a mixture of redox active species of A and B with properties listed in Table 1 and redox potential of $E_0^A = -0.5\,V\ vs.SHE\ and\ E_0^B = -0.5, -0.55, -0.6, -0.65, -0.7\ , -0.8, -0.9\,V\ vs.SHE$. a) Half-cell potentials of the mixtures during both reduction and oxidation. b) the Average of the reduction and oxidation half-cell potentials at different potential separations.

So far, we presented the data for redox active compounds mixed with equal concentrations. **Figure S1a** presents the voltage-capacity profiles for a case where different ratios of A (-0.5 V vs. SHE) and B (-0.8 V vs. SHE) are mixed. Depending on the relative concentrations, the onset of the second voltage plateau during reduction/oxidation can be shifted to the left or right. When all the properties of A and B are identical except for the redox potential, the average voltage during charge-discharge simply follows the rule of mixtures (**Figure S1b**).

The results shown so far were obtained by assuming equal kinetic and mass-transfer properties for compounds A and B. If such properties are dissimilar then the results can change significantly: for example, the benefit of having compound B with large negative redox potential or large solubility could be completely negated if compound B has a significantly lower mass transfer or reaction kinetic rate constant. In **Figure 4**, we show simulated results of a mixture of 60% compound A (-0.5 V vs. SHE) and 40% B (-0.8 V vs. SHE) subjected to constant-current cycling with voltage limits. **Figure 4a** shows the cell potential vs. capacity for different magnitudes of the mass-transfer rates (different $k_{m,B}$ values) of compound B and **Figure 4b** shows the resulting voltage efficiency of the cell assuming the negolyte is paired with a hypothetical posolyte with the same standard reduction potential of ferricyanide/ferrocyanide, +0.47 V vs. SHE, but with arbitrarily large volume so that the posolyte SOC remains at 50% as the negolyte is charged and discharged. Additionally, the accessed capacity in the negolyte extracted from Figure 4a is shown. As the mass-transfer coefficient of compound B drops, approaching $< 10^{-6}$ m s^{-1}, not only does the average half-cell potential drop, but also the accessed capacity of the cell within the chosen voltage window drops. Specifically, when the mass-transfer coefficient reaches $k_{m,B} = 6.5\times10^{-8}$ m s^{-1}, the round-trip voltage efficiency (RTVE) of the battery decreases to 54%. This reduction in efficiency is significant, as it brings the performance on par with an unmixed solution containing only compound A. Consequently, the presence of compound B, which initially resulted in a higher voltage efficiency, becomes practically indistinguishable from using compound A alone. Furthermore, at this mass-transfer coefficient, the accessed capacity is restricted to only 83% of the total capacity. This means that the battery can store and deliver only a fraction of its maximum potential charge. If the mass-transfer coefficient further drops below 6.5×10^{-8} m s^{-1}, the voltage efficiency experiences an even greater decline, falling below that of compound A. Additionally, the accessed capacity is significantly limited, further exacerbating the constraints imposed on the system.

Similarly, **Figure 4c-d** presents the effect of exchange current difference for the same example. Indeed, for slower exchange current density of compound B, the portion of the capacity that is delivered by compound B would have a higher overpotential and thus the round-trip voltage efficiency decreases as depicted in **Figure 4d** for the example where the mixed negolyte is paired with ferrocyanide/ferricyanide redox reaction. The round-trip voltage efficiency becomes on par with the voltage efficiency of an unmixed solution of pure A when the exchange current of

compound B drops below 6.0×10^{-4} mA. A fivefold decrease in the exchange current of B resulted in a reduction in voltage efficiency by 4 percentage points.

As such, if a redox active species is added to a mixture in our electrolyte to bring a certain attractive property (e.g., increasing cell voltage or solubility), we should make sure that the gain from the desired benefit is not undermined by the low kinetic or mass transfer rate of the added compound.

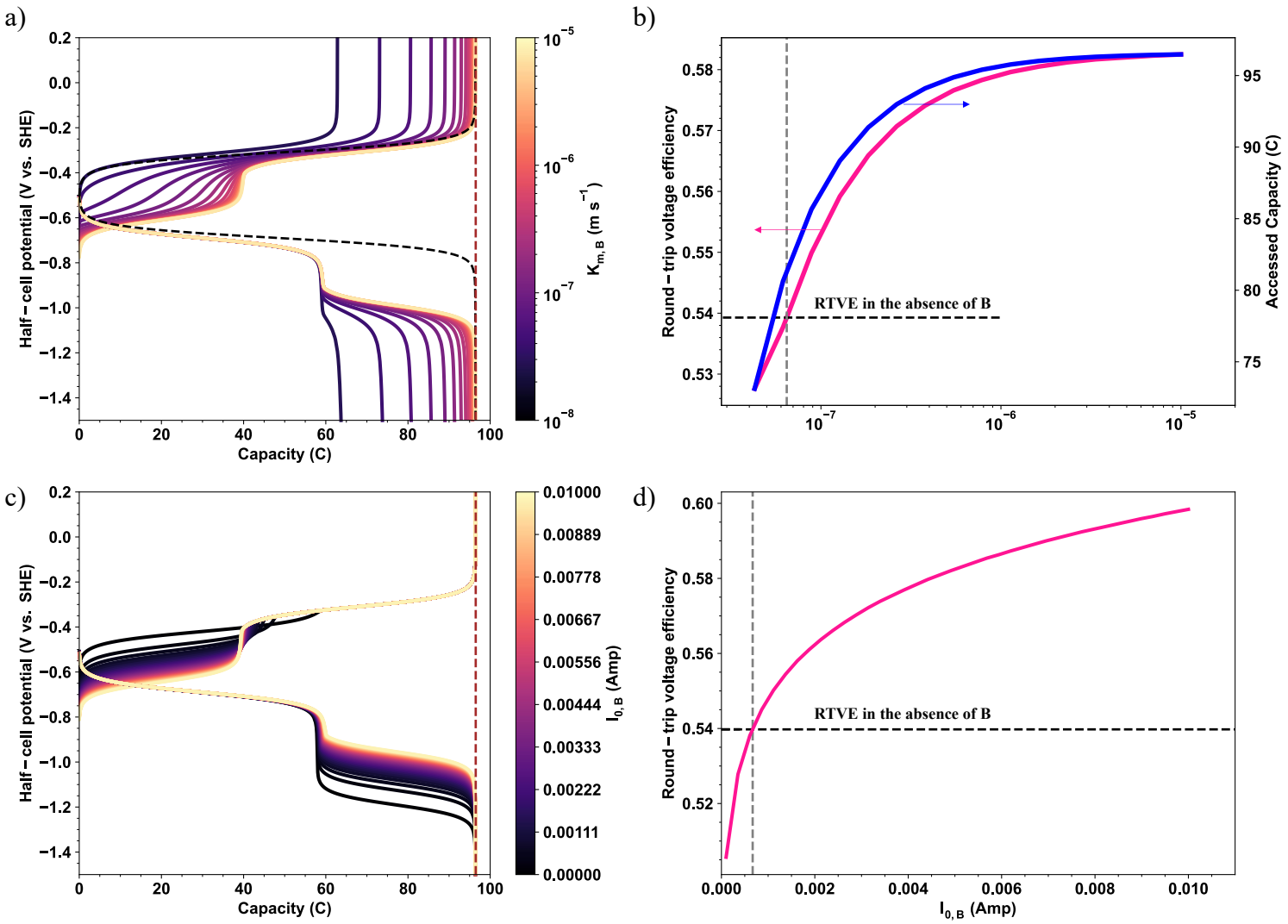

Figure 4 Simulated properties of a mixture of redox active species of A (-0.5 V vs. SHE) and B (-0.8 V vs. SHE) with different mass-transfer coefficients (top) and different exchange currents (bottom). a) and b) illustrate the voltage vs. capacity, the accessed capacity under galvanostatic cycling, and the voltage efficiency against the hypothetical posolyte discussed in the text for different mass-transfer coefficients of B when the mass-transfer coefficient of A is held at 10^{-5} m s^{-1}. The simulations were performed for mass-transfer coefficients ranging from 4.0E-08 to 1.00E-05 with regular increments. The increment between consecutive coefficients was ~2 times the previous value.; c) and d) illustrate the voltage vs. capacity and the voltage efficiency for

different exchange currents of B when the exchange current of A is held at 5×10^{-3} A. The exchange current densities were incrementally varied within the range of 0.0001 to 0.01. A total of 40 equally spaced values were used for this increment.

Thus far, we presented the modeling results in the absence of a homogenous redox reaction. Because the redox active species are mixed in the tank, the chemical reaction (Reaction 15) can take place. Note that this chemical reaction does not change the total available capacity, implying that the delivered capacity and coulombic efficiency of the battery are not affected by the reaction. The voltage efficiency of the battery, however, should be affected by this chemical reaction as low-potential (high-energy) species spontaneously transfer their capacity to higher-potential (lower-energy) species. The direction of this chemical reaction is a function of the concentration of A and B (battery SOC) and the potential separation between their redox potentials; the rate depends additionally on the kinetic rate constant for the homogeneous reaction and, possibly, the kinetic rate constant for a heterogeneous chemical reaction catalyzed by electrolyte-contacting surfaces including the electrode itself.

Figures 5a depicts the concentration of an equi-molar mixture of A and B ($E_0^A = -0.5\,V\,SHE, E_0^B = -0.6\,V\,SHE$) with 100 mV potential separation between their redox potentials, charged to 50% SOC. We assume that, after completing the charging process, the battery is held at 50% SOC long enough for chemical equilibrium to be established, with the equilibrium constant dictated by the separation in their redox potentials. The increase in the concentration of B^{2+} and the decrease in the concentration of A^{2+} is shown in **Figures 5a** which shows that the equilibrium has pushed the reaction (15) in the forward direction. **Figure 5b** reports the charge-discharge voltage-capacity curves of the same mixture when charged to and held at three different SOC values with (solid line) and without (dashed line) a chemical reaction. At SOC of 80%, virtually no effect is observed in the discharge voltage curve while at lower SOCs, a drop is observed. This is because at 80% SOC, the majority of A^{2+} is already reduced and thus a reaction quotient is found which is slightly higher than the equilibrium constant (K = 49 at 100 mV separation), pushing the reaction slightly to the left. **Figure 5c** shows the concentration of reduced species A^+ and B^+ with and without a chemical reaction at different SOC values. It is clear that at each SOC, the total concentration of reduced species before and after the chemical reaction has not changed – only the fraction of the B^+ and A^+ in the total reduced species has changed. At 20% and 50% SOC the concentration of B^+ has dropped by 86% and 50%, respectively, but at 80% SOC the concentration of B^+ is slightly increased by 4%. A drop of 86% in the concentration of species B may seem substantial but, because it constituted only a small fraction of the total concentration, its impact is minor. The fraction of concentration of B^+ in the total reduced concentration at different SOCs and potential separations is shown in **Figure 5d**. Note that potential separations up to only 200 mV is presented here because the results reported in Figure 2a and 2b show that at potential separations above a threshold of approximately 200 mV, the compound A is essentially completely reduced by the time the reduction of B^{2+} begins. Consequently, above this potential separation, the homogenous redox reaction occurrence is minimal. Similar to the case of 100 mV potential separation, for 50 mV and 200 mV separation,

the B^+ fraction has slightly increased at 80% SOC. At 20% SOC, the fraction of B^+ has dropped from 0.35 to 0.17 for 50 mV potential separation and from 0.07 to 0 for 200 mV potential separation.

Figure 5e shows the resulting round-trip voltage efficiency loss (in terms of the percent of the reaction-free RTVE) at different SOC and potential separations, assuming the hypothetical ferrocyanide/ferricyanide posolyte. The highest voltage efficiency loss was 2.35% of the reaction-free RTVE, which was found at 20% SOC and 100 mV separation. The voltage efficiency losses for different potential separations demonstrate a clear trend of decreasing as the SOC at the end of charging increases. This behavior arises from the intricate interplay between the concentrations of the higher and lower energy species in their reduced and oxidized forms. For instance, at 20% SOC and a potential separation of 100 mV, the concentrations of A^{2+}, A^{+}, B^{2+} and B^{+} are 68.3, 31.7, 90.9, and 9.1 M respectively. These concentrations result in a reaction quotient that is 10 times lower than the equilibrium constant. Consequently, the forward reaction (15) is favored, leading to an 86% decrease in the concentration of B+, the high-energy species. At 50% SOC, the concentrations of A^{2+}, A^{+}, B^{2+} and B^{+} are 23.16 M, 76.8 M, 74.73 M and 25.20 M, respectively. This configuration yields a reaction quotient 4.5 times lower than the equilibrium constant, resulting in a 46% reduction in the concentration of B+. Comparing the losses in the high-energy species between 20% SOC and 50% SOC, it becomes apparent that the voltage efficiency loss is higher at 20% SOC for the case of a 100 mV separation. Another noteworthy observation from Figure 5e is the distinct point at which the voltage efficiency drops to zero for different potential separations. Specifically, there is a smooth decline to zero at 70% SOC for a 50 mV separation, in contrast to an abrupt drop at 54% SOC for 200 mV separation, correlated with the complete loss in the oxidized form of the lower-energy species (A^{2+}) depicted in Figure 2c discussed previously.

Although at a high potential separation of 200 mV the equilibrium constant is high and the forward reaction is highly favoured, the voltage efficiency loss is low because at higher separations, lower concentration of A^{2+} can co-exist with B^+ at each SOC (see Figure 2). Thus, the concentration changes as a result of the reaction (15) are small. Conversely, at lower potential separations between compounds A and B, the reduction reactions of A and B occur more simultaneously, enabling higher concentrations of A^{2+} to coexist with B^+ at each SOC. However, as the potential separation decreases, the tendency for the chemical reaction decreases as well (indicated by lower K), leading to a diminishing impact on the voltage efficiency loss. Consequently, the interplay between the potential separation between compound A and B and the concentration ratios mitigates the extent of voltage efficiency loss, making it relatively insignificant for the case of equi-molar mixture of species with identical properties other than their potential separation.

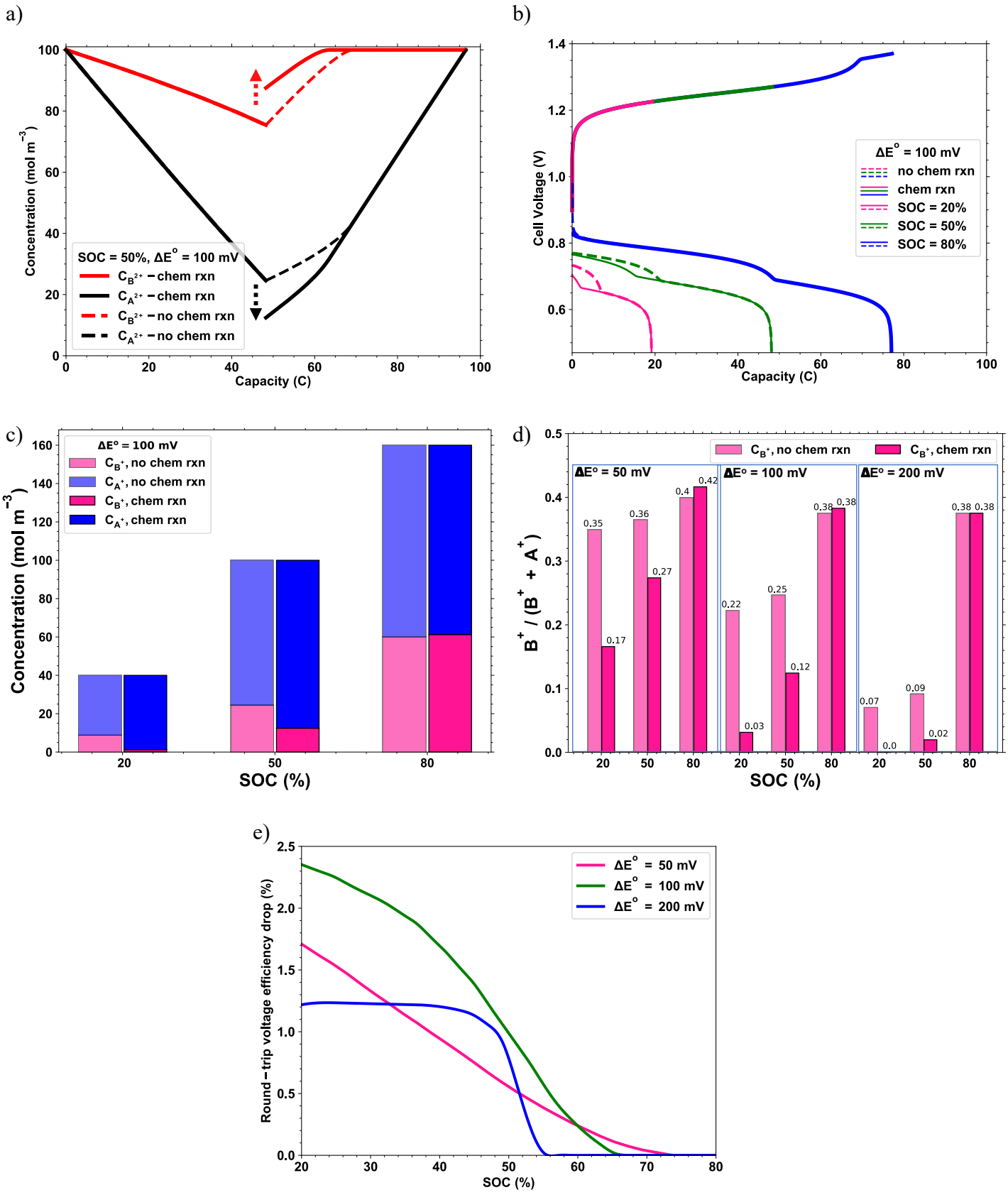

Figure 5 a) Simulated concentrations of A^{2+} and B^{2+} versus capacity for an equi-molar mixture of

A (-0.5 V vs. SHE) and B (-0.6 V vs. SHE) charged to 50% SOC. The solid line shows the concentrations when sufficient time is given after charge for the chemical reaction to reach equilibrium. The dashed lines show the results in the absence of a chemical reaction. b) Voltage-capacity, assuming a hypothetical ferrocyanide/ferricyanide posolyte operating at a SOC-invariant redox potential of +0.47 V vs. SHE, for the same mixture charged to 20%, 50% or 80% SOC in the presence and absence of a chemical reaction. c) Concentration of A^+ and B^+ at different SOCs before and after a chemical reaction. d) Fraction of reduced species of B in the total concentration at different SOCs and potential separations. e) Round-trip voltage efficiency loss assuming a hypothetical ferrocyanide/ferricyanide posolyte operating at a SOC-invariant redox potential of +0.47 V vs. SHE, in terms of percent of the reaction-free voltage efficiency, vs. SOC at various potentials separations.

Experimental Case Study

Experimental Details

Chemicals

Analytical grade reagents and deionized water were used for preparing all solutions. Reagents used were potassium ferrocyanide trihydrate, potassium ferricyanide, potassium hydroxide (all purchased from Sigma Aldrich) and 2,6-DHAQ (2,6-Dihydroxyanthraquinone), 2,6-DPPEAQ (((9,10-dioxo-9,10-dihydroanthracene-2,6-diyl)bis(oxy))bis(propane-3,1-diyl))bis(phosphonic acid) purchased from TCI Chemicals and 1,5-DHAQ (1,5-Dihydroxyanthraquinone) purchased from Fisher Scientific. 2,6-N-TSAQ was synthesized following the synthesis route in our previous work [14]. Henceforth, we abbreviate 2,6-DPPEAQ as DPPEAQ and 2,6-N-TSAQ as N-TSAQ. Furthermore, we further abbreviate 2,6-DHAQ as DHAQ, except when it is important to distinguish it from 1,5-DHAQ.

Cyclic Voltammetry

Cyclic voltammetry was recorded by a Gamry potentiostat with a three-electrode system including one glassy carbon working electrode, one platinum counter electrode and one Ag/AgCl reference electrode. The glassy carbon working electrode was polished with an aluminum slurry before and after each scan.

Flow Battery Experiments

Cell components from Fuel Cell Technologies Inc. (Albuquerque, NM), or in-house cells with PVC end plates were employed for flow battery experiments. Interdigitated flow fields made up of pyrosealed POCO graphite flow plates were used in each half cell of the battery with 3 layers of baked (400 ^{o}C overnight) carbon paper (SGL 39AA) per side. The torque applied during cell assembly (for cells from Fuel Cell Technologies Inc.) was 60 lb-in (6.78 N·m) on each of eight

3/8”–24 bolts, thus the load applied per bolt is approximately 800 lbs. For the in-house cells, this torque was 18 1b-in on each of eight 3/8”–24 bolts. The geometric area of each electrode was 5 cm^2. The two half-cells were separated by a Nafion 212 cation-exchange membrane and a Viton sheet (10 mils) as a gasket. All membranes were soaked in 1 M KOH for over a day before operation. The electrolytes were pumped into the cell using either KNF FF12 diaphragm pumps (for low concentration tests) or peristaltic pumps (for high concentration tests) using fluorinated ethylene propylene (FEP) tubing with a flow rate of 60 ml/min. The cells were operated inside a nitrogen-filled glovebox. Cycling tests were conducted by employing the constant current followed by constant voltage (CCCV) protocol.

NMR measurements

^{1}H NMR is employed to study whether the two water-soluble AQs in the mixed electrolyte can react and generate new decomposition compounds apart from what have been identified in their isolated electrolytes. The NMR samples were prepared as described previously [12] . 100 μL aliquots were taken from the electrolytes and diluted with 550 μL D_2O to afford the resulting solutions. The solutions were stored in normal NMR tubes. Aeration was conducted for the fully reduced electrolytes before NMR measurements. The ^{1}H NMR data were collected at room temperature with 32 scans from Bruker AVANCE NEO 400.

Overview of DHAQ and N-TSAQ Redox-Active Compounds

For the purpose of this case study, we have chosen two of the previously reported anthraquinones, namely, 2,6-dihydroxyanthraquinone (2,6-DHAQ) [15] and sodium 3,3',3",3"'-((9,10-anthraquinone-2,6-diyl)bis(azanetriyl))tetrakis(propane-1-sulfonate) (2,6-N-TSAQ) [14], as candidates for exploring the performance of their mixture. The individual properties of these species make them reasonable candidates for constructing a mixed redox-active solution. DHAQ has an acceptable operating concentration limit at 0.5 M, equivalent to 1 M of transferrable electrons. Nevertheless, in the absence of an electrochemical recovery of its degradation products [22], DHAQ demonstrates a fast capacity fade rate of 4-8%/day. N-TSAQ, in contrast, has a lower operating concentration limit at 0.35 M, but is two orders of magnitude more stable than DHAQ, with a fade rate of 0.025%/day [14]. By preparing a mixture of these two molecules, not only do we expect to achieve a higher volumetric energy density, but we also expect to achieve it with an overall fade rate lower than 4-8%. This is because part of the extra energy density achieved will be provided by N-TSAQ, which is a more stable compound compared to DHAQ.

Cyclic Voltammetry

Figure 6a presents the cyclic voltammetry of individual solutions of 10 mM DHAQ and 10 mM N-TSAQ dissolved in 1 M KOH as well as a mixture of 10 mM DHAQ + 10 mM N-TSAQ in 1 M KOH. The two compounds show close redox potentials, with 55 mV difference

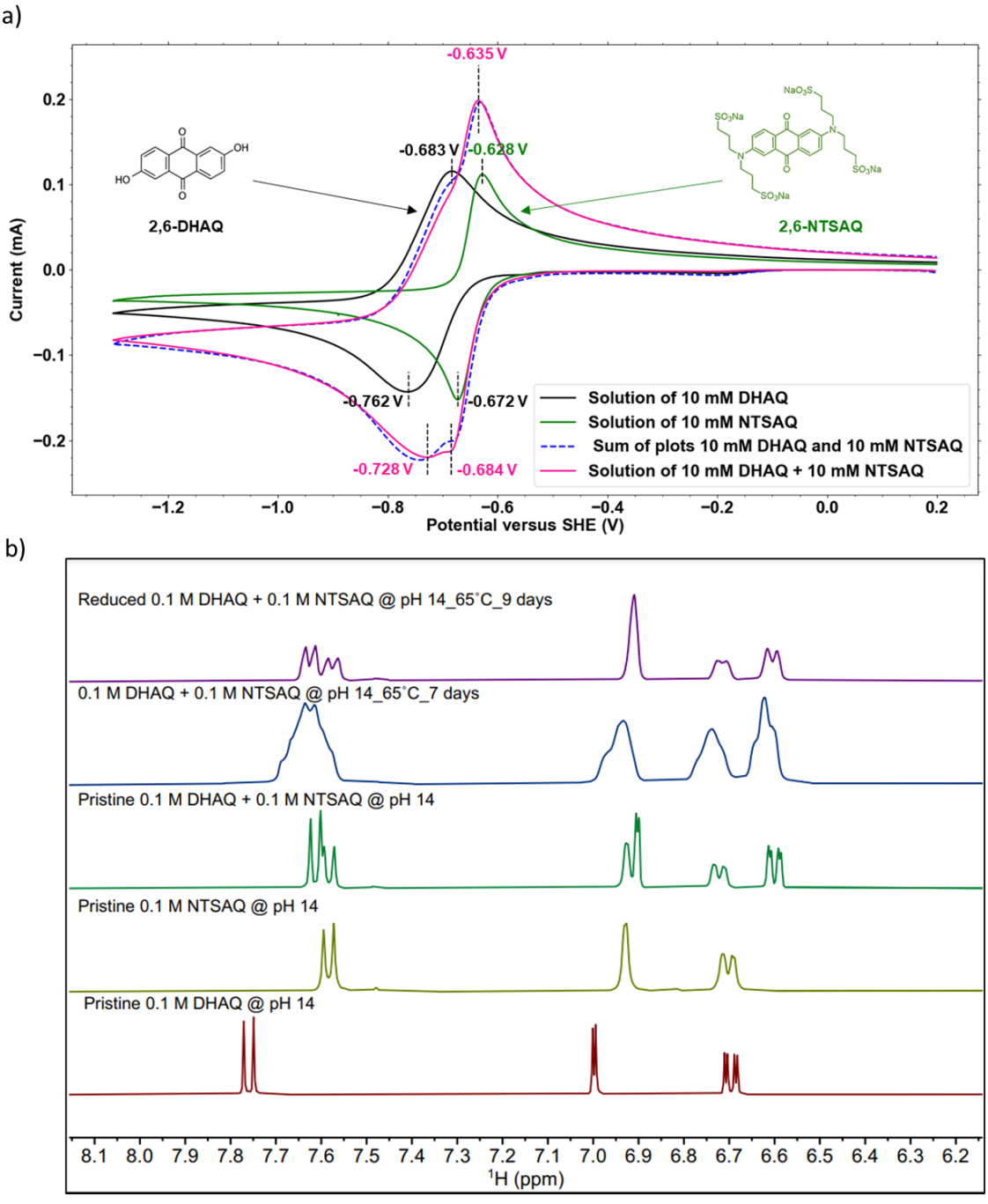

Figure 6 a) Cyclic voltammetry profiles of 10 mM DHAQ in 1 M KOH, 10 mM N-TSAQ in 1 M KOH and a mixture of 10 mM DHAQ + 10 mM N-TSAQ in 1 M KOH. For comparison, the sum of the individual cyclic voltammetry plots of 10 mM DHAQ and 10 mM N-TSAQ is also shown. All cyclic voltammetry profiles are background corrected. b) ^{1}H NMR spectra of pristine solutions

of oxidized form of 0.1 M DHAQ, 0.1 M N-TSAQ and mixture of 0.1 M DHAQ + 0.1 M N-TSAQ at pH 14. Additionally, the ^{1}H NMR of the reduced and oxidized forms of 0.1 M DHAQ + 0.1 M N-TSAQ mixture after storage at 65 ^{o}C for 7 days is shown. For every NMR sample preparation, we added 550 μL of D_2O to a 100 μL of pH 14 electrolyte, then transferred it to a NMR tube.

between their oxidation peaks and 90 mV separation between their reduction peaks. As is evident from the cyclic voltammetry profile of their mixture, the two reduction potentials of the compounds show a doublet reduction peak with 44 mV separation. Additionally, the oxidation peak of the compounds in the mixture is merged into almost one single peak, with a shoulder at -0.684 V. Given that the concentration of the mixed solution is twice the concentration of each individual solution, and the redox potential of the individual redox-active species are close, the higher current delivered from the mixed solution as well as the presence of merged reduction and oxidation peaks is not a surprise, as is indicated by the similarity of the CV trace for the mixed species and the sum of the CV traces of the individual species.

Chemical Stability

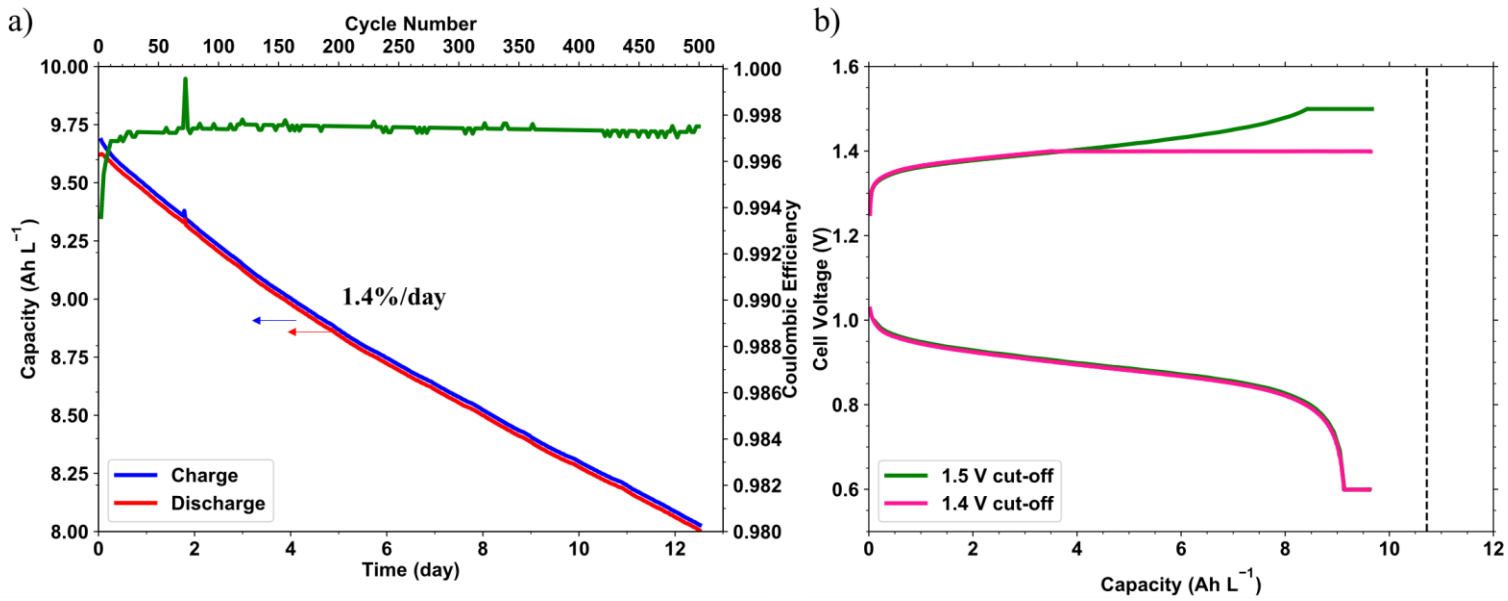

Figure 7: Long term cell cycling of a redox flow battery operated with a constant current (40 mA cm^{-2}) followed by constant potentials of 1.4 V (charging) and 0.5 V (discharging) during 12 days of operation at room temperature. The cell was assembled with a mixture of 5 mL 0.1 M N-TSAQ + 0.1 M DHAQ in 1 M KOH paired with 50 mL of 0.2 M ferrocyanide + 0.06 M ferricyanide in 1 M KOH separated by a Nafion 212 cation exchange membrane. The cell cycling tests are conducted in a N_2-filled glove box. The capacity is presented in units of Ampere-hours per liter of

negolyte. a) Charge and discharge capacities and coulombic efficiency versus time (b) Charge-discharge voltage-capacity profiles of the battery at two different cut-off voltages of 1.4 V and 1.5 V.

To investigate whether, by mixing N-TSAQ and DHAQ anthraquinones, new degradation paths become viable, first the proton NMR spectra of the pristine isolated solutions of each compound, each in its oxidized state, are compared to that of their mixed solution. In **Figure 6b**, the aromatic protons (7.4-7.8 ppm) of the two AQ derivatives at pH 14, which have slightly different chemical shifts in the isolated solutions, partially overlap in the pristine mixed solution. Although the peak broadening of the mixed solution in its oxidized state after the thermal treatment suggests the existence of molecular interaction, the absence of new peaks indicates there is no new molecular decomposition compound generated by the thermal treatment. The spectrum of the fully reduced mixed solution after the thermal treatment and aeration also shows no appreciable decomposition compound peaks. Hence there appears to be no new decomposition pathways occurring in the mixed electrolytes. It is worth noting that the chemical shifts in the mixed electrolyte NMR spectrum do not appear to be the sum of the chemical shifts of the two pristine individual spectra, which is due to the difference in concentration of total organic molecules [23] or the slight difference in pH introduced while diluting the electrolytes with D_2O for the NMR sample preparation [24].

To quantify the degradation rate of the mixture and quantitively examine whether the fade rate would accelerate as the result of mixing these two anthraquinones, we operated a flow battery with 5 mL 0.1 M N-TSAQ + 0.1 M DHAQ in 1 M KOH paired with 50 mL 0.2 M ferrocyanide + 0.06 M ferricyanide potassium salts in 1 M KOH for over 12 days with a CCCV protocol at 40 mA cm^{-2} with voltage cut-off values of 1.4 V and 0.6 V. N-TSAQ and DHAQ are reported to separately demonstrate capacity fade rates of 0.025%/day [14] and 4-8%/day [15], respectively. As such, in a one-to-one mixture of these two compounds and in the absence of any change in the individual decomposition rates, a fade rate between 2.5%/day and 4%/day is expected. As shown in **Figure 7a**, the mixed solution of N-TSAQ and DHAQ exhibited an overall fade rate of 1.4%/day (see also Figure S2), which is even lower than the fade rate expected based on those of the individual compounds. This suggests that the possibility of increased stability of the less stable compound upon mixing warrants further investigation. Nevertheless, the important conclusion for the present case study is that the mixing of these two anthraquinones in the same electrolyte shows no evidence of accelerating their degradation rates; hence there appears to be no trade-off of stability vs. volumetric capacity. The theoretical accessible capacity based on total of 0.2 M concentration of the mixture is 10.72 Ah L^{-1} and the accessed capacity percentage in this test was 90%. We attribute the difference between the realized capacity and the theoretical value to the presence of redox-inactive impurities and errors in electrolyte volume measurement. The prior work on N-TSAQ, using the same synthesis route, showed an accessed capacity percentage of 88%, whereas the accessed capacity percentage for DHAQ has been typically close to 95%. Given these values, the

accessed capacity in the present test is also typical and does not suggest any abnormal immediate loss in capacity upon mixing. Furthermore, as shown in **Figure 7a**, the coulombic efficiency of the battery remains very high and stable at >99.7% throughout the 12 days of experiment, demonstrating the insignificance of any side reactions during operation. **Figure 7b** shows the voltage versus capacity of the battery at two different charge voltage cut-offs. As the two compounds possess close redox potentials, there is no discernible separation of voltage plateaus during the charge or discharge phases of the battery. This analysis demonstrates that a battery with mixture of N-TSAQ and DHAQ in the negolyte shows no sign of accelerated degradation or side reactions and could be effectively used in the present case study.

Addressing Motivation 1: Increasing the Volumetric Energy Density

Because mixing the two molecules did not accelerate the degradation of the mixed redox-active negolyte, we used the mixture at higher concentrations as a case study for addressing our first motivation: increasing the volumetric energy density of the battery. A flow battery was assembled with 7 mL of 0.2 M N-TSAQ + 0.5 M DHAQ in 1 M KOH paired with 100 mL 0.2 M sodium ferrocyanide + 0.1 M potassium ferrocyanide + 0.1 potassium ferricyanide in 1 M KOH and operated with CCCV protocol at 40 mA cm^{-2} with voltage cut-off values of 1.4 V and 0.6 V. In this case, the negolyte total concentration is 0.7 M, which should yield 40% higher volumetric energy density than the isolated solution of DHAQ at its maximum operating concentration of 0.5 M and 100% higher than N-TSAQ at its maximum operating concentration of 0.35 M. Based on fades rates of 0.025%/day and 4-8%/day for separate solutions of N-TSAQ and DHAQ, respectively, a fade rate between 2.9%/day and 5.7%/day is expected when the mixture is created with 0.2 M N-TSAQ + 0.5 M DHAQ. **Figure 8a** presents the charge and discharge capacities and the coulombic efficiencies for almost 10 days of operation. As can be seen, an overall fade rate of 2.5 ± 0.84%/day is exhibited with a coulombic efficiency of 99%. Note that the semi-log plot of the capacity versus time in Figure S2b shows two regions with slightly different slopes and thus the fade rate is reported based on the average of the fade rates of the two regions. The expected theoretical capacity of the negolyte is 37.5 Ah L^{-1}, 91% of which was accessed. These results demonstrate the successful increase of the volumetric energy density without a sacrifice in the fade rate. Note that while DHAQ dissolves easily in 1 M KOH, it forms a paste in 1 M NaOH even at the low concentration of 0.1 M. Because the N-TSAQ synthesized in the present work has sodium counter ions, we did not create a mixture with both compounds at their maximum solubility, (0.5 M DHAQ + 0.35 M N-TSAQ). In principle, however, preparing N-TSAQ with a potassium counter ion should enable further increases beyond 40% in the volumetric energy density.

Addressing Motivation 2: Bringing Low-Solubility Redox-Active Species Back into the Material Discovery Cycle

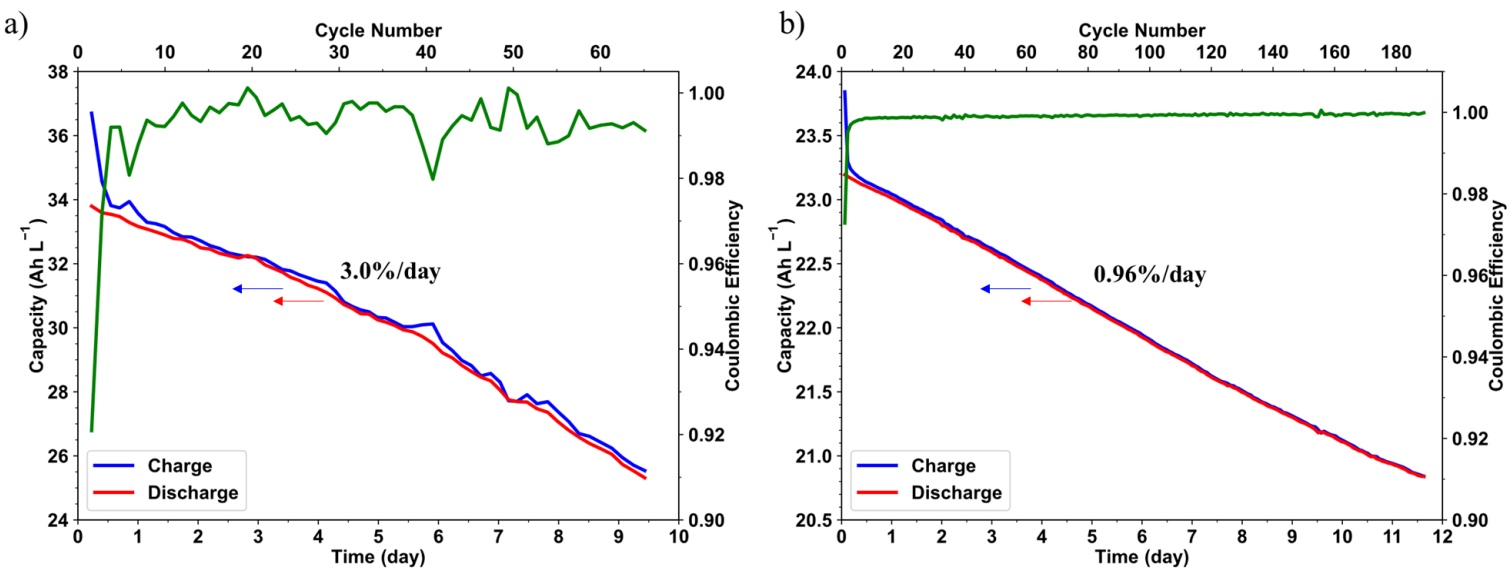

Figure 8 a) Long term cell cycling of a redox flow battery assembled with a mixture solution of 7 mL of 0.2 M N-TSAQ + 0.5 M DHAQ in 1 M KOH paired with 100 mL 0.2 M sodium ferrocyanide + 0.1 M potassium ferrocyanide + 0.1 M potassium ferricyanide in 1 M KOH separated by a Nafion 212 cation exchange membrane. b) Long term cell cycling of a redox flow battery assembled with 5 mL of a mixture of 0.35 M N-TSAQ + 0.15 M DHAQ in 1 M KOH paired with 50 mL 0.4 M potassium ferrocyanide and 0.1 M potassium ferricyanide in 1 M KOH separated by a Nafion 212 cation exchange membrane. For both experiments, the cell cycling tests are conducted in a N_2-filled glove box. The capacity is presented in units of Ampere-hours per liter of negolyte.

Given that N-TSAQ has an operating concentration limit of 0.35 M, the compound might be left out of the material discovery cycle for not meeting our minimum desired operating concentration of 0.5 M for a compound with 2 electron transfer. However, considering the mixed redox active strategy, one can be less strict about the solubility limits of newly designed redox active organic species. For example, as shown in **Figure 8b**, we have raised the operating concentration of the battery to the minimum desired operating concentration of 0.5 M by mixing 0.35 M N-TSAQ with 0.15 M DHAQ in 1 M KOH, yielding a total of 0.5 M solubility. Based on the individual fade rates of each compound and the ratios of their concentrations, a fade rate of 1.2%/day – 2.4%/day is expected for 0.35 M N-TSAQ + 0.15 M DHAQ in 1 M KOH mixture, and the experimentally exhibited fade rate is only 0.96%/day (**Figure 8b** and **Figure S2**). These results demonstrate that a compound with a low solubility, but otherwise other interesting properties, may still be viable for use in RFBs because the mixed redox active strategy could transcend the solubility threshold for useful deployment.

Possibility of Occurrence of a Homogenous Chemical Reaction and its Relationship with Redox Potential Separation and SOC

The results of the modeling section showed that, for small potential separations, the oxidized form of the compound with a more positive redox potential can be present simultaneously with the reduced form of the compound with a more negative redox potential in significant amounts, depending on the SOC of the battery. Consequently, the homogenous redox reaction described by Eq. (15) is possible in the tank. Beyond a certain, property-dependent redox potential separation, however, the modeling results suggest that these species do not coexist in significant amounts and, consequently, we expect no homogenous redox reaction between the mixed species in the system.

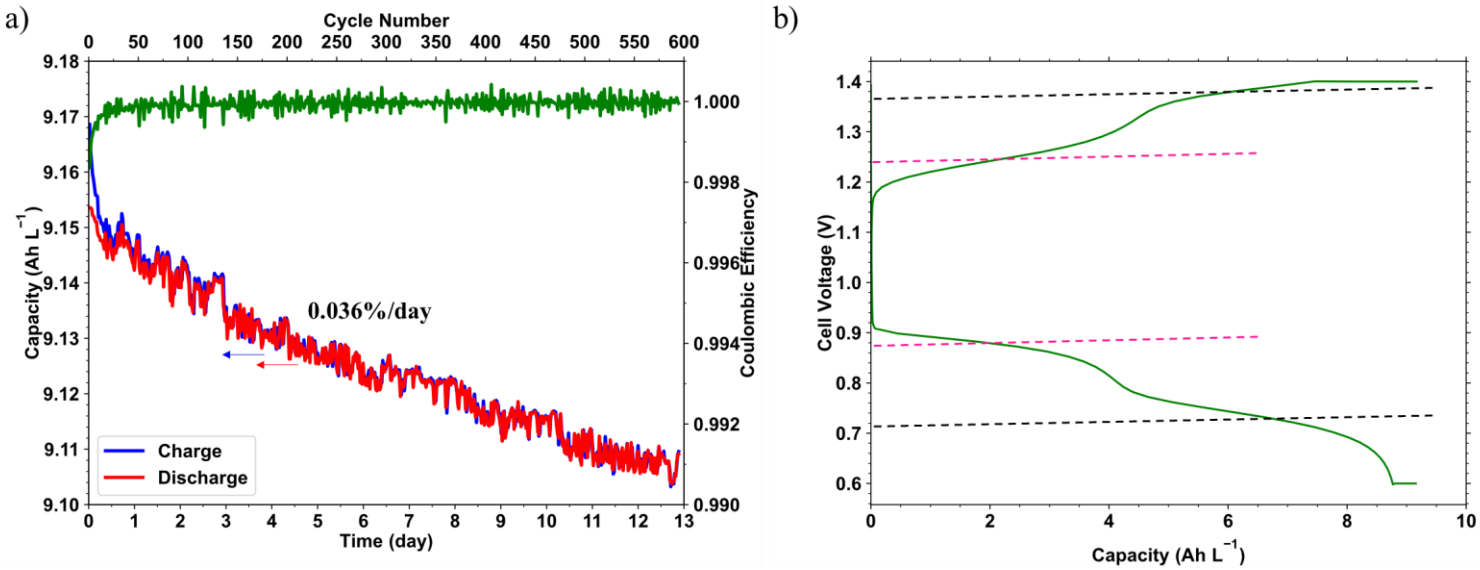

Figure 9 a) Long term cell cycling of a redox flow battery assembled with 5 mL of a mixture of 0.1 M N-TSAQ + 0.1 M DPPEAQ in 1 M KOH paired with 50 ml 0.2 M ferrocyanide + 0.06 M ferricyanide in 1 M KOH separated by Nafion 212. b) Cell voltage versus capacity of the cell.

In order to study this chemical reaction and its relationship with SOC and the potential separation of the mixture of species, two experimental cases are examined. The first case is the already-discussed mixture of N-TSAQ and DHAQ with a potential separation of 72 mV, where we expect the possibility of a homogenous redox reaction over a certain SOC range. For the second case, we study a mixture of DPPEAQ and N-TSAQ, with a potential separation of 232 mV. The mixture of 0.1 M DPPEAQ + 0.1 M N-TSAQ at pH 14 has been operated against 0.2 M ferrocyanide + 0.06 M ferricyanide in 1 M KOH for more than 12 days to investigate their chemical stability in the presence of one another. The charge and discharge capacity, coulombic

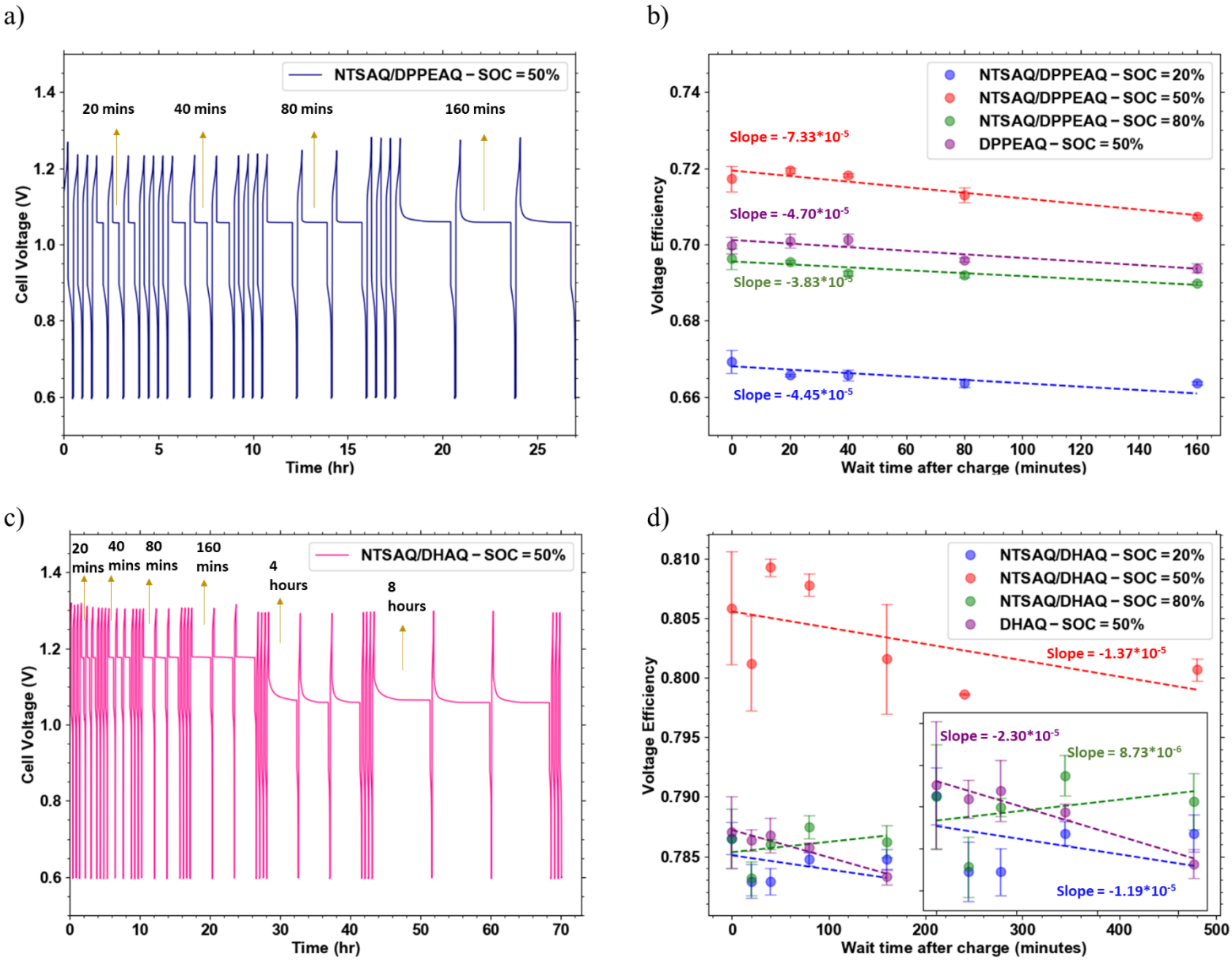

Figure 10 Wait-time experiments for investigation of self-discharge in mixture of 0.1 M N-TSAQ + 0.1 M DPPEAQ in 1M KOH (a and b) and 0.1 M N-TSAQ + 0.1 M DHAQ (c and d) in 1M KOH. In all cases the volume of the negolyte was 5 mL and the posolyte was 50 mL of 0.2 M ferrocyanide and 0.1 M ferrocyanide in 1 M KOH. a) and c) voltage versus time profiles, indicating alternating cycles with no wait after discharge (3 cycles each time) and different durations of waiting (3 cycles each time). b) and d) Round-trip voltage efficiency versus cycle number.

efficiency, and the voltage-capacity profile of this mixed-negolyte cell are shown in **Figure 9**. Given the individual fade rates of the mixture (0.07 ± 0.02 %/day for DPPEAQ and 0.025%/day for N-TSAQ), the fade rate of 0.036%/day achieved for the mixture is at the low end of the expected range of 0.0475± 0.01%/day, demonstrating no acceleration in the chemical stability as a result of mixing. The voltage-capacity profile clearly shows the presence of two plateaus, indicated by horizontal dashed lines, because of the large separation between the potentials of the two compounds.

For characterization of the homogenous redox reaction in these two mixtures, the battery was first operated normally for 5 cycles, meaning that the discharge phase immediately followed the charging phase. Afterward, for 5 cycles, the battery was charged at 20 mA cm^{-2} to a certain SOC (20%, 50% and 80%) and a wait-time of 20 minutes was added before the discharging phase began. This was repeated for wait times of 40 minutes, 80 minutes and 160 minutes. This procedure was used to characterize a homogeneous redox reactionfor iron complexes [25]. The experiment was also repeated for separated solutions of DPPEAQ and DHAQ, for comparison.

Figure 10a and **Figure 10c** show the results of these experiments at 50% SOC. We determined the round-trip voltage efficiency of the cell at each cycle number for each of the SOC restrictions tested (see **Figure S3**). **Figure 10b** and **Figure 10d** depict the average round-trip voltage efficiency for each of the wait-time durations and at different SOCs of 20%, 50% and 80% for mixtures of N-TSAQ/ DPPEAQ and N-TSAQ/ DHAQ, respectively. It should be emphasized that the important criteria that need to be compared are the changes of voltage efficiency between different wait times within the same SOC restriction. The voltage efficiency should not be compared across different SOC experiments or different compositions because small ohmic drop differences should affect the voltage efficiency across tests.

Figure S4 shows the zoomed images of each individual test for N-TSAQ/DPPEAQ and **Figure 10b** summarizes the results for N-TSAQ/DPPEAQ in a single figure. The poor fit between the line of best fit and the data displayed in **Figure S4** indicates that the correlation between the duration of the wait time and the voltage efficiency is weak. The slope of these lines is almost horizontal, with a value in the range of -10^{-5} per minute. These slopes are comparable to that of the control experiment conducted with the separated solution of DPPEAQ. Lack of a significant drop in the voltage efficiency for this mixture is consistent with our expectation that a large potential separation between the two compounds (230 mV in this case) suppresses the coexistence of the oxidized form of the species with the higher redox potential and the reduced form of the species with the lower redox potential.

For the case of N-TSAQ + DHAQ, with a potential separation of only 72 mV, we indeed expect that the oxidized form of N-TSAQ to be present simultaneously with the reduced form of the DHAQ and thus the occurrence of chemical reaction is possible. Given the small potential separation of the compounds, however, the thermodynamic driving force should be small. As

shown in **Figure 10d**, there is not a significant discernible correlation between voltage efficiency at different wait time durations. The lines of best fit show slopes in the range of 10^{-5} – 10^{-6} per minute, similar to the control experiment with separated solution of DHAQ. The chemical reaction phenomenon is expected to occur more significantly at 20% SOC and 50% SOC where high concentrations of both oxidized NTSAQ and reduced DHAQ are simultaneously present. Nevertheless, we see no correlation between the slope of the fitted lines across states of the charge of the cell. The results obtained in this section demonstrate that even in scenarios where the simultaneous existence of the oxidized form of a less negative compound and the reduced form of a more negative compound is anticipated, the occurrence of a chemical homogenous redox reaction may not have a significant impact on the system. However, it is important to note that the voltage efficiency loss needs to be studied on a case-by-case basis. Multiple molecular interactions, such as steric and Coulombic forces, can impact on the homogeneous chemical reaction between the mixed molecules and the resulting voltage efficiency loss.

Design Guideline for Mixed Redox-Active Systems

Based on the present study, the following points should be considered for the design of mixed redox active organic electrolyte:

- The mixture may be designed with a goal of achieving a certain volumetric capacity that is inaccessible to the individual solutions of desirable redox-active species. For example, multiple low-soluble, but otherwise low-cost, stable redox active species can be mixed to create a practical battery electrolyte.

- Individual properties of the redox-active species such as kinetic rate constant and, for electrolyte/electrode combinations, mass transfer coefficient, must be taken into account. For example, if one of the redox reactions in the mixture has sluggish kinetics or slow mass transfer, the voltage efficiency of the overall system would be affected, as well as, when the battery is operated in the galvanostatic mode, the accessed capacity.

- The chemical stability of the redox active species in the mixture should be studied in order to assess possible interactions among different species. Comparing the temporal fade rate and accessed fraction of theoretical capacity of the mixture with the same properties for each species individually is recommended.

- The occurrence of a homogenous redox reaction in the mixture and its effect on the voltage efficiency loss in the battery needs to be considered. This chemical reaction is expected to be prevented at very small potential separations (where ΔG becomes small) or at potential separations higher than a threshold dictated by species properties (where co-existence of

the charged and uncharged forms of the two species is prevented). Intermediate potential separations must be studied in a case-by-case basis. According to the 0D model, for an equi-molar mixture of redox active species with 1 electron transfer, the rate should be low when the redox potential difference is greater than ~200 mV. Interactions not captured by the 0D model, e.g. coexistence within the electrode and flow field during operation, may promote such reactions beyond the extent captured by the 0D model. Note that the electrode potential of organic species can be tuned by structural modification and thus optimization for achieving desirable potential separations is possible.

- Viscosity of the solutions designed with high volumetric energy density must be taken into account. High-concentration organics may increase the viscosity to such an extent that redesign of the porous electrode and flow field is necessary to suppress pumping losses.

Although in the present study we intentionally prepared systems with mixed redox-active molecules, the learning points are directly applicable to systems for which, at the beginning of operation, a single redox active molecule is present, but through chemical degradation, essentially a mixture of redox active species is formed during operation. For example, it has been shown that dimerization occurs in the posolyte of RFBs with $Fe(Bhmbpy)_3$ and $Fe(bpy)_3$ redox active metalorganic compounds [25]. Over time, this results in a mixture of the original iron complex and a redox active dimer with a less positive redox potential. As such, the electrolyte can be viewed as a mixture of two redox active species and scrutinized with methods presented in the present work. In addition, although we report a case study on the mixture of different redox active molecules, the concepts can be extended to mixtures of isomers of the same redox active molecule, which tend to have similar redox potentials. Remarkably, our solubility measurements show that whereas 1,5-DHAQ has a solubility of only 0.09 M in 1 M KOH, its solubility is more than doubled to 0.25 M when mixed with 0.45 M 2,6-DHAQ, yielding a total of 0.7 M concentration (**Figure S5**). The use of isomer mixtures appears to be a very promising research direction for increasing volumetric capacity.

Conclusion

In this study, we employ computational and experimental methods to analyze the electrochemical performance of mixed redox-active organic molecules with the goal of enhancing the volumetric capacity of an aqueous-soluble organic electrolyte beyond the solubility limit of a single species. To achieve this, we utilize a 0-dimensional transient model that assumes uniform compositions throughout and neglects the electrolyte composition in the remaining plumbing. We investigate the changes in temporal concentration profiles, partial currents, and half-cell potential of a mixture comprising two redox reactions. Furthermore, we discuss the influence of individual properties of each compound, including their kinetic and mass transfer rates, redox potentials, and concentration

ratios. The model shows that when the standard redox potentials of the two equi-molar mixed species, A and B, are separated by more than approximately 200 mV, the species with the higher redox potential undergoes near-complete conversion before the species with the lower redox potential experience significant conversion. This prevents the occurrence of an energy-losing spontaneous homogeneous chemical redox reaction between the charged and uncharged forms of the two species. In cases where the standard redox potentials of A and B in a mixture are separated by less than about 200 mV, and their molar ratio and the electrolyte state of charge fall within a specific range, determined by the kinetic rate constants for the heterogeneous redox reaction at the electrode and the mass transfer coefficients of the species within the electrode, the aforementioned homogeneous chemical redox reaction becomes a possible energy loss mechanism, leading to a decrease in round-trip voltage efficiency. However, numerical solutions indicate that the loss in the round-trip voltage efficiency in such instances over a complete charge-discharge cycle is relatively small for an equi-molar mixture. In our experimental investigations, we combine DHAQ and N-TSAQ, resulting in a mixture that exhibits a volumetric capacity 40% higher than that achievable by the more soluble species alone. Moreover, our examination of binary mixtures of DHAQ, N-TSAQ, and DPPEAQ at a dilute concentration of 0.1 M reveals that mixing does not adversely affect the capacity fade rates of the mixtures and the wait-time experiments reveal insignificance voltage efficiency loss for DHAQ/N-TSAQ and DPPEAQ/N-TSAQ pairs. Based on our modeling and analysis of the experimental results, we propose guidelines for designing suitable mixed redox-active organic species.

Acknowledgments

This research was supported by the National Science Foundation through grant CBET-1914543 and by U.S. DOE award DE-AC05-76RL01830 through PNNL subcontract 535264. K.A. was supported in part through the Natural Sciences and Engineering Research Council of Canada (NSERC) Postdoctoral Fellowship (PDF) program [application number PDF - 557232 – 2021]. The authors also thank Eric Fell, Thomas George, Dawei Xi, Abdul Alfaraidi, Daniel Pollack, Kyumin Lee, Taobo Wang and Sophia Edgar for valuable discussions.

Conflict of Interest

M.J.A. acknowledges a significant financial stake in Quino Energy, Inc., which might profit from the results reported here. All other authors declare no conflict of interest.

References

[1]J. Rugolo and M.J. Aziz, "Electricity Storage for Intermittent Renewable Sources", *Energy & Environmental Science* **5**, 7151 (2012). https://doi.org/https://doi.org/10.1039/C2EE02542F

[2]Z. Zhu, T. Jiang, M. Ali, Y. Meng, Y. Jin, Y. Cui, and W. Chen, "Rechargeable Batteries for Grid Scale Energy Storage", *Chemical Reviews* (2022).

[3]A.Z. Weber, M.M. Mench, J.P. Meyers, P.N. Ross, J.T. Gostick, and Q. Liu, "Redox Flow Batteries: A Review", *Journal of Applied Electrochemistry* **41**, 1137 (2011). https://doi.org/10.1007/s10800-011-0348-2

[4]D.G. Kwabi, Y. Ji, and M.J. Aziz, "Electrolyte Lifetime in Aqueous Organic Redox Flow Batteries: A Critical Review", *Chem Rev* **120**, 6467 (2020). https://doi.org/10.1021/acs.chemrev.9b00599

[5]Y. Li, Z. Xu, Y. Liu, S. Jin, E.M. Fell, B. Wang, R.G. Gordon, M.J. Aziz, Z. Yang, and T. Xu, "Functioning Water-Insoluble Ferrocenes for Aqueous Organic Flow Battery Via Host–Guest Inclusion", *ChemSusChem* **14**, 745 (2021). https://doi.org/ https://doi.org/10.1002/cssc.202002516

[6]W. Wu, J. Luo, F. Wang, B. Yuan, and T.L. Liu, "A Self-Trapping, Bipolar Viologen Bromide Electrolyte for Redox Flow Batteries", *ACS Energy Letters* **6**, 2891 (2021). https://doi.org/https://doi.org/10.1021/acsenergylett.1c01146

[7]E.S. Beh, D. De Porcellinis, R.L. Gracia, K.T. Xia, R.G. Gordon, and M.J. Aziz, "A Neutral Ph Aqueous Organic–Organometallic Redox Flow Battery with Extremely High Capacity Retention", *ACS Energy Letters* **2**, 639 (2017). https://doi.org/https://doi.org/10.1021/acsenergylett.7b00019

[8]S. Pang, X. Wang, P. Wang, and Y. Ji, "Biomimetic Amino Acid Functionalized Phenazine Flow Batteries with Long Lifetime at near-Neutral Ph", *Angewandte Chemie International Edition* **60**, 5289 (2021). https://doi.org/https://doi.org/10.1002/anie.202014610

[9]J. Xu, S. Pang, X. Wang, P. Wang, and Y. Ji, "Ultrastable Aqueous Phenazine Flow Batteries with High Capacity Operated at Elevated Temperatures", *Joule* **5**, 2437 (2021). https://doi.org/https://doi.org/10.1016/j.joule.2021.06.019

[10]K. Lin, R. Gómez-Bombarelli, E.S. Beh, L. Tong, Q. Chen, A. Valle, A. Aspuru-Guzik, M.J. Aziz, and R.G. Gordon, "A Redox-Flow Battery with an Alloxazine-Based Organic Electrolyte", *Nature Energy* **1**, 1 (2016). https://doi.org/10.1038/nenergy.2016.102

[11]Z. Li, T. Jiang, M. Ali, C. Wu, and W. Chen, "Recent Progress in Organic Species for Redox Flow Batteries", *Energy Storage Materials* (2022).

[12]K. Amini, E.F. Kerr, T.Y. George, A.M. Alfaraidi, Y. Jing, T. Tsukamoto, R.G. Gordon, and M.J. Aziz, "An Extremely Stable, Highly Soluble Monosubstituted Anthraquinone for Aqueous Redox Flow Batteries", *Advanced Functional Materials* (2023). https://doi.org/10.1002/adfm.202211338

[13]E.F. Kerr, Z. Tang, T.Y. George, S. Jin, E.M. Fell, K. Amini, Y. Jing, M. Wu, R.G. Gordon, and M.J. Aziz, "High Energy Density Aqueous Flow Battery Utilizing Extremely Stable, Branching-Induced High-Solubility Anthraquinone near Neutral Ph", *ACS Energy Letters* **8**, 600 (2022). https://doi.org/10.1021/acsenergylett.2c01691

[14]M. Wu, M. Bahari, Y. Jing, K. Amini, E.M. Fell, T.Y. George, R.G. Gordon, and M.J. Aziz, "Highly Stable, Low Redox Potential Quinone for Aqueous Flow Batteries", *Batteries & Supercaps* e202200009 (2022). https://doi.org/https://doi.org/10.26434/chemrxiv-2021-rjzdn).

[15]K. Lin, Q. Chen, M.R. Gerhardt, L. Tong, S.B. Kim, L. Eisenach, A.W. Valle, D. Hardee, R.G. Gordon, and M.J. Aziz, "Alkaline Quinone Flow Battery", *Science* **349**, 1529 (2015).

[16]S. Agnew and P. Dargusch, "Consumer Preferences for Household-Level Battery Energy Storage", *Renewable and Sustainable Energy Reviews* **75**, 609 (2017). https://doi.org/10.1016/j.rser.2016.11.030

[17]S. Park, H.J. Lee, H. Lee, and H. Kim, "Development of a Redox Flow Battery with Multiple Redox Couples at Both Positive and Negative Electrolytes for High Energy Density", *Journal of The Electrochemical Society* **165**, A3215 (2018). https://doi.org/10.1149/2.0301814jes

[18]Z.N. Wei Wang, Baowei Chen, Feng Chen, Qingtao Luo, Yuyan Shao, Xiaoliang Wei, Guan-Guang Xia, Liyu Li, Zhenguo Yang, "A New Hybrid Redox Flow Battery with Multiple Redox Couples", presented at the 221st ECS Meeting, 2012 (unpublished).

[19]S. Corcuera and M. Skyllas-Kazacos, "State-of-Charge Monitoring and Electrolyte Rebalancing Methods for the Vanadium Redox Flow Battery", *European Chemical Bulletin* **1**, 511 (2012). https://doi.org/https://doi.org/10.1016/j.jpowsour.2011.06.080

[20]Y. Cao, C.T. Ser, M. Skreta, K. Jorner, N. Kusanda, and A. Aspuru-Guzik, "Reinforcement Learning Supercharges Redox Flow Batteries", *Nature Machine Intelligence* **4**, 667 (2022). https://doi.org/10.1038/s42256-022-00523-2

[21]B.J. Neyhouse, A.M. Fenton, and F.R. Brushett, "Too Much of a Good Thing? Assessing Performance Tradeoffs of Two-Electron Compounds for Redox Flow Batteries", *Journal of The Electrochemical Society* **168**, (2021). https://doi.org/10.1149/1945-7111/abeea3

[22]Y. Jing, E.W. Zhao, M.-A. Goulet, M. Bahari, E.M. Fell, S. Jin, A. Davoodi, E. Jónsson, M. Wu, and C.P. Grey, "In Situ Electrochemical Recomposition of Decomposed Redox-Active Species in Aqueous Organic Flow Batteries", *Nature Chemistry* 1 (2022). https://doi.org/https://doi.org/10.6084/m9.figshare.19612128

[23]P.J.S. Abhijit Mitra, b R. Ali A~sarpoti, Thomas Williamsonb "Unprecedented Concentration Dependent Chemical Shift Variation in 'H-Nmr Studies: A Caveat in the Investigations of Molecular Recognition and Structure Elucidation ", *Tetrahedron* **54**, 15489 (1998).

[24]M.A. Goulet, L. Tong, D.A. Pollack, D.P. Tabor, S.A. Odom, A. Aspuru-Guzik, E.E. Kwan, R.G. Gordon, and M.J. Aziz, "Extending the Lifetime of Organic Flow Batteries Via Redox State Management", *J Am Chem Soc* **141**, 8014 (2019). https://doi.org/10.1021/jacs.8b13295

[25]J. Gao, K. Amini, T.Y. George, Y. Jing, T. Tsukamoto, D. Xi, R.G. Gordon, and M.J. Aziz, "A High Potential, Low Capacity Fade Rate Iron Complex Posolyte for Aqueous Organic Flow Batteries", *Advanced Energy Materials* **12**, (2022). https://doi.org/10.1002/aenm.202202444